

1 **A CMIP6 ensemble for downscaled monthly climate normals over** 2 **North America**

3 Colin R. Mahony^{1*}, Tongli Wang², Andreas Hamann³, and Alex J. Cannon⁴

4

5 1. British Columbia Ministry of Forests, Lands, Natural Resource Operations and Rural
6 Development, Victoria, BC, Canada.

7 2. Centre for Forest Conservation Genetics, Department of Forest and Conservation
8 Sciences, Faculty of Forestry, University of British Columbia, Canada

9 3. Department of Renewable Resources, Faculty of Agricultural, Life, and Environmental
10 Sciences, University of Alberta, Canada

11 4. Climate Research Division, Environment and Climate Change Canada, Victoria, British
12 Columbia, Canada

13 *Correspondence to colin.mahony@gov.bc.ca; twitter @ColinRMahony

14

15 **Abstract**

16 Many studies of climate change impacts and adaptation use climate model projections
17 downscaled at very high spatial resolution (~1km) but very low temporal resolution (20- to 30-
18 year normals). These applications have model selection priorities that are distinct from analyses
19 at high temporal resolution. Here, we select a 13-model CMIP6 ensemble designed for robust
20 change-factor downscaling of monthly climate normals and describe its attributes in North
21 America. The ensemble is representative of the distribution of equilibrium climate sensitivity and
22 grid resolution in the CMIP6 generation. We provide rationale for an 8-member subset of the
23 ensemble based on screening criteria and sequence these 8 models for selection of smaller
24 ensembles for regional analysis. Although we have focused our documentation on North
25 America, the 13-model ensemble is selected using global criteria and applicable to downscaling
26 climate normals in other continents. Downscaled projections for the selected models are
27 available in ClimateNA (<http://climatena.ca/>), An accompanying web application ([https://bcgov-
28 env.shinyapps.io/cmip6-NA/](https://bcgov-env.shinyapps.io/cmip6-NA/)) provides tools for further model selection and visualization of the
29 ensemble.

30

31 **Keywords:** Climate change, downscaling, model selection, CMIP6, North America.

32

33 1 Introduction

34 The most recent iteration of the Coupled Model Intercomparison Project (CMIP6; Eyring
35 et al. 2016) is a once-in-a-decade update to projections of climate change. CMIP6 provides a
36 larger number of simulations from a new generation of global climate models, at higher spatial
37 resolution, and using an improved set of emissions scenarios relative to its predecessor, CMIP5
38 (Taylor et al. 2012). These new climate simulations contribute to and are put into broader context
39 by the Sixth Assessment Report from Working Group I of the Intergovernmental Panel on
40 Climate Change (Lee et al. 2021). CMIP6 simulations are rapidly being incorporated into
41 downscaled climate data products for use in regional climate change impacts and adaptation
42 initiatives. These initiatives can benefit from careful selection of climate model projections that
43 are suited to broad classes of end uses, and their wide application requires transparency on the
44 attributes of these ensembles.

45 Many climate change impact analyses, particularly in ecology, use projections of climate
46 change that are downscaled to very high resolution (~1km) but very low temporal resolution (20-
47 to 30-year climate normals). The prevalence of this type of analysis is evident from the
48 widespread use of WorldClim (Hijmans et al. 2005, Fick and Hijmans 2017; 23340 citations) and
49 ClimateNA (Wang et al. 2012, 2016, Hamann et al. 2013; 1678 citations). The low temporal
50 resolution of these applications simplifies downscaling; both WorldClim and ClimateNA use
51 change-factor downscaling, also called the climate imprint method (Hunter and Meentemeyer
52 2005) and simple mean bias correction (Maraun 2016). This method adds low-spatial-resolution
53 anomalies from the climate model to a high-resolution gridded climate map (Tabor and Williams
54 2010). The best practices for change-factor downscaling to high-spatial and low-temporal
55 resolution are different than those for the more sophisticated statistical downscaling techniques
56 necessary for high temporal resolution downscaling (Wilby et al. 2004), leading to distinct model
57 selection priorities.

58 One consideration in model selection for change-factor downscaling is the number of
59 simulation runs for each candidate model. The change-factor method is sensitive to the influence
60 of natural variability in the historical reference period against which anomalies are calculated
61 and bias correction is applied. Similarly, natural variability during the projected future periods
62 adds “noise” to the climate change “signal” (Hui et al. 2020), the latter being of primary interest
63 to analyses of projected climate normals. Performing change-factor downscaling with multiple
64 simulations runs of each model reduces the confounding influence of natural variability in bias
65 correction and improves the signal-to-noise ratio (Milinski et al. 2019). Consequently, models
66 with multiple simulations for each historical and future scenario are preferable in this context.

67 Another consideration is the model bias. All climate models exhibit biases--systematic
68 differences between observations and simulations—at the regional scale. Removal of these
69 biases is a basic step in downscaling (Maraun 2016). Change-factor downscaling performs
70 univariate bias correction and therefore may not conserve the physical (e.g., thermodynamic)
71 interdependence between variables such as temperature and precipitation (Cannon 2018). The
72 associated potential for univariate downscaling to produce physically implausible climatic
73 conditions presumably increases with the size of the biases in the simulation. For this reason,
74 models with small biases are preferable to models with large biases, all else being equal.

75 Finally, the spatial resolution of climate models is of interest to high spatial resolution
76 downscaling. Some models contributing to the CMIP6 ScenarioMIP (O'Neill et al. 2016)
77 experiment (the candidate pool for ensemble selection in this study) have horizontal grid
78 resolutions of 70-100km. These medium-resolution models are able to resolve macrotopography,
79 e.g., to differentiate the major mountain ranges of the Western Cordillera. The opportunity to
80 better represent the influences of water bodies and topography on climate change trends, such as
81 elevation-dependent warming (Salathé et al. 2008, Palazzi et al. 2019), is appealing for climate
82 change impact analyses. Conversely, models with very low spatial resolution (>300km) can
83 conflate the climate change signals of distinct regions, particularly at land/ocean transitions
84 (Lanzante et al. 2018). Very low resolution therefore is a consideration for exclusion from
85 ensembles designed for high-resolution change-factor downscaling.

86 Collectively, the three considerations described above suggest an ensemble that prioritizes
87 number of simulations per model rather than number of models, low-to-moderate bias, and
88 moderate-to-high spatial resolution.

89 Once a general-purpose ensemble is selected, it is useful to structure the ensemble for
90 further user-specific model selection. Many applications of projected climate normals are
91 computationally intensive analyses at regional scales. In these cases, it can be desirable to use a
92 small number (3-8) of models that represent the approximate range of a more comprehensive
93 ensemble. Cannon (2015) describes a method for structuring an ensemble into an order of subset
94 selection that optimally represents the ensemble spread. Alternatively, analysts may wish to
95 select a custom subset of the ensemble. Documentation of the attributes of the ensemble
96 members can help analysts to identify subsets that are best suited to specific applications.

97 The purpose of this study is to select and describe an ensemble of CMIP6 model
98 projections of 21st century climate change over North America. The focus of model selection is
99 on facilitating robust downscaling of projected climate normals at very high spatial resolution.
100 We characterize the attributes, biases, and climate change trends of the ensemble and highlight
101 features of interest in individual climate models. Finally, we provide ordered subsets of the
102 ensemble for regional analyses and considerations for selection of custom subsets. Downscaled
103 projections for the selected 13 CMIP6 models are available in ClimateNA (<http://climatena.ca/>),
104 which provides downscaling at user-specified spatial resolution and various temporal intervals
105 (annual, 20-year and 30-year periods). An accompanying web application ([https://bcgov-
106 env.shinyapps.io/cmip6-NA/](https://bcgov-env.shinyapps.io/cmip6-NA/)) provides tools for further model selection and visualization of the
107 ensemble.

108 2 Methods

109 2.1 Criteria for model selection

110 We assessed all models in the ESGF holdings for the CMIP6 ScenarioMIP as of December
111 15, 2020. We selected models using six objective criteria, listed below with rationale:

- 112 • **Criterion 1: T_{\min} and T_{\max} available.** Mean daily minimum temperature (T_{\min}) and
113 mean daily maximum temperature (T_{\max}) are the directly measured elements of the long-

114 term temperature record, and are the fundamental temperature elements in many climate
115 change impact analyses.

- 116 • **Criterion 2: Minimum of 3 historical runs available.** This criterion ensures robust
117 downscaling by reducing the confounding influence of natural variability in bias
118 correction.
- 119 • **Criterion 3. Complete scenarios.** Models need to have at least one simulation for three
120 of the four major SSP marker scenarios (SSP1-2.6, SSP2-4.5, SSP3-7.0, and SSP5-8.5).
- 121 • **Criterion 4. One model per institution.** This criterion is a widely applied best practice
122 in ensemble selection (Leduc et al. 2016) as one measure to increase independence
123 among ensemble members. For the purposes of this criterion, different physics or forcing
124 schemes of the same model were considered different models.
- 125 • **Criterion 5. No closely related models.** Models that share components were excluded,
126 following Figure 5 of Brunner et al. (2019).
- 127 • **Criterion 6. No large biases.** Bias is the degree to which a model simulation differs
128 from the observed climate over a reference period (1961-1990 in this case). Models with
129 large biases relative to the rest of the ensemble in one or more variables were excluded.

130 2.2 *Ensemble subset criteria*

131 Users of the ensemble may wish or need to use a lesser number of models in their analyses.
132 To support the selection of subsets, we structure the ensemble by defining an order of exclusion
133 of models. Models are excluded in two phases: first based on screening criteria to exclude
134 models with lower value for the anticipated uses of the ensemble, and second using the method
135 of Cannon (2015) to represent the range of climate changes in the remaining models.

136 2.2.1 *Screening criteria*

137 Priority for exclusion from model subsets was established using four screening criteria.
138 The screening criteria are more subjective than the six selection criteria defined above. They
139 generally are not sufficient in isolation but combinations of the criteria provide some justification
140 for model exclusions.

- 141 • **Criterion 7. Constraints on equilibrium climate sensitivity (ECS).** Multiple lines of
142 evidence indicate that the Earth's equilibrium climate sensitivity (ECS) is *likely*
143 (probability > 66%) between 2.5°C and 4°C and *very likely* ($p > 90\%$) between 2°C and
144 5°C (Sherwood et al. 2020, Arias et al. 2021). The evidence is robust for the lower bound,
145 and weaker for the upper bound. From one perspective, inclusion of models with ECS
146 outside this very likely range biases the multi-model ensemble mean and unnecessarily
147 increases the modeling uncertainty in downstream analyses (Ribes et al. 2021). An
148 alternate perspective is that high-sensitivity models are useful as a representation of high-
149 impact, low-likelihood scenarios (Sutton and Hawkins 2020). To accommodate both
150 perspectives, we provide structured subsets with and without high-sensitivity models.

- 151 • **Criterion 8. Model resolution.** Some ScenarioMIP models have sufficiently high spatial
152 resolution to resolve macrotopography, e.g., to differentiate the major mountain ranges of
153 the Western Cordillera. These models are weighted towards inclusion in the ordered
154 subsets. Models with very low spatial resolution are weighted towards exclusion in the
155 subset.
- 156 • **Criterion 9. Number of simulation runs.** The ensemble is designed for analysis of
157 projected climate normals; the climate change signal is of primary interest. In this
158 context, internal variability of the models is a confounding factor, producing erratic
159 climate change trajectories in noisy climate variables like precipitation and winter
160 temperature. The signal-to-noise ratio can be increased by averaging the projected
161 normals over multiple simulations of the same emissions scenario. Models with only one
162 run are weighted for exclusion.
- 163 • **Criterion 10: Grid cell artefacts.** Models exhibiting spatially anomalous climate
164 changes in individual grid cells are problematic for many of the intended uses of this
165 ensemble, and are weighted for exclusion from the structured subsets.

166 2.2.2 *Ordered subsets*

167 After exclusion of models using the screening criteria above, an order of exclusion for the
168 remaining models is defined using the Katsavounidis–Kuo–Zhang (KKZ) algorithm, using the
169 application to climate model ensemble selection described by Cannon (2015). KKZ
170 deterministically selects models that best represent the spread of multivariate climate changes
171 projected by the ensemble. KKZ subset selection is ordered, starting with the model closest to
172 the ensemble centroid, and incrementally adding models to a region of the ensemble variation
173 that is poorly represented by each successive subset.

174 Since the spatial patterns of climate change differ among models, we provide separate
175 KKZ subsets for each of the seven IPCC climate reference regions (Iturbide et al. 2020) within
176 North America. We also provide an ordered subset for North America as a whole, but caution
177 that ensembles of less than 8 models are likely insufficient to represent spatial variation in
178 modeling uncertainty at continental scales (Pierce et al. 2009, McSweeney et al. 2014, Cannon
179 2015). The implementation of KKZ in this study used the mean of the z-standardized seasonal
180 changes in T_{\min} , T_{\max} , and precipitation in four consecutive 20-year time periods starting with
181 2021-2040 and three emissions scenarios (SSP1-2.6, SSP2-4.5, and SSP3-7.0).

182 2.3 *Analysis of model bias*

183 We assessed model bias as *mean absolute bias* over North America in each monthly
184 climate variable. For each grid cell, i , the mean simulated 1961-1990 climate normal of the K
185 historical model runs, f_{ik} is calculated as

$$\bar{f}_i = \frac{1}{K} \sum_{k=1}^K f_{ik} \quad (1)$$

186 The absolute value of the difference between the simulated 1961-1990 normal, \bar{f}_i , and the
187 observed 1961-1990 normal, o_i , aggregated onto the native model grid is calculated for each grid
188 cell:

$$|e_i| = |\bar{f}_i - o_i| \quad (2)$$

189 The mean absolute bias, $|e|$, over all N projected grid cells in North America is calculated as:

$$|e| = \frac{1}{N} \sum_{i=1}^N |e_i| \quad (3)$$

190 To equalize the area of grid cells, we projected absolute bias in the native model grid onto a
191 Lambert Conformal Conic grid with 0.5° resolution prior to calculating this mean.

192 For precipitation variables, Equations 1 and 2 were performed on log-transformed normals.
193 Subsequent to Equation 3, this log-transformation was reversed by taking the exponent of
194 absolute bias. Doing so expresses absolute bias of precipitation as a factor of magnitude. e.g.,
195 simulated precipitation normals of 50% and 200% relative to observed precipitation both have an
196 absolute bias of 2.

197 **2.4 Cluster analysis**

198 For visualization of similarity among models, we perform a standard cluster analysis on six
199 climate variables (minimum temperature, maximum temperature, and precipitation for winter
200 and summer) at 325 locations (by resampling all models to a common 300 km resolution). To
201 reduce dimensions for clustering, we used three principal components instead of the original six
202 variables, resulting in 975 variables for the construction of the dendrogram (325 locations x 3
203 principal climate components). We used Ward's hierarchical clustering algorithm with a
204 Euclidean distance of standardized principal components (i.e., a Mahalanobis distance metric),
205 implemented with the hclust package for the R programming environment.

206 **3 Results**

207 **3.1 Ensemble selection**

208 There were 44 models in the CMIP6 ScenarioMIP holdings as of December 15, 2020
209 (Table 1). Twelve of these candidates were excluded because they did not provide monthly
210 means of T_{\min} and T_{\max} (Criterion 1). Notably, CESM2 does provide T_{\min} and T_{\max} in its future
211 projections, but due to an archiving error these variables are not available for historical runs. An
212 additional eleven models were excluded because they had less than three historical runs
213 (Criterion 2) or an incomplete scenario set (Criterion 3). Of the 21 models that passed these first
214 three strict criteria, we excluded two more models on the basis of having a clear choice between
215 models from the same institution (Criterion 4): CanESM5-CanOE in favour of CanESM5; and
216 EC-Earth3-Veg in favour of EC-Earth3. In addition, of the several variants of the GISS-E2-1-G
217 model, we selected the r*i1p3f1 variant because it had the most complete set of scenario
218 simulations. We downloaded historical simulations from the remaining 19 models for further

219 evaluation. For practical purposes, we limited downloads to 5 historical simulations for EC-
220 Earth3 due to its relatively high resolution, and 10 simulations for other models.

221 To assist with choosing among models from the same institution (Criterion 4) or with
222 shared components (Criterion 5), we conducted an analysis of bias in T_{\min} , T_{\max} , and
223 precipitation (PPT) (Figure 1). We excluded AWI-CM-1-1-MR on the sole basis of its very high
224 temperature bias (Criterion 6). NESM3 also has high bias relative to the other models, and
225 excluded due to shared components with MPI-ESM1 (Criterion 5). None of the other related
226 models were distinct from each other in terms of bias.

227 Final choices from among related models were: UKESM1.0-LL selected over HadGEM3-
228 GC31-LL due to higher resolution and more simulations; MIROC6 over MIROC-ES2L due to
229 higher number of runs and regionally high biases in the Pacific Northwest; MPI-ESM1.2-HR
230 over MPI-ESM1-2-LR to improve representation of high-resolution models in the ensemble; and
231 CNRM-ESM2-1 arbitrarily selected over CNRM-CM6-1 in favour of the ESM configuration. In
232 summary, the six criteria reduced the 44 candidate models to a 13-model ensemble (Table 2).

233 **Table 1: Candidate models, model exclusion criteria, and number of simulation runs.** Model list and
 234 number of simulations per scenario are ESGF holdings as of December 15, 2020. ECS is equilibrium
 235 climate sensitivity (long-term temperature change in response to an instant doubling of CO₂); ECS values
 236 are quoted from Meehl et al. (2020). See Table 1 for citations and institutions of selected models.

Model	Criterion for exclusion	ECS	ESGF holdings					Analyzed				
			historical	ssp126	ssp245	ssp370	ssp585	historical	ssp126	ssp245	ssp370	ssp585
ACCESS-CM2	2 <3 historical runs	4.7	2	1	1	1	1					
ACCESS-ESM1-5		3.9	30	10	30	10	10	10	10	10	10	10
AWI-CM-1-1-MR	6 very high bias	3.2	5	1	1	5	1	3				
BCC-CSM2-MR		3.3	3	1	1	1	1	3	1	1	1	1
CAMS-CSM1-0	1 No tmax/tmin	2.3	3	2	2	2	2					
CESM2	1 No tmax/tmin in historical	5.2	11	3	3	3	3					
CESM2-WACCM	1 No tmax/tmin in historical	4.8	3	1	5	3	5					
CIESM	3 incomplete scenarios		3	1			1					
CMCC-CM2-SR5	1 No tmax/tmin		1	1	1	1	1					
CNRM-CM6-1	4 same institution	4.9	30	6	10	6	6	10				
CNRM-CM6-1-HR	2 <3 historical runs	4.3	1	1	1	1	1					
CNRM-ESM2-1		4.8	11	5	10	5	5	11	5	5	5	5
CanESM5		5.6	65	50	50	50	50	10	10	10	10	10
CanESM5-CanOE	4 same institution		3	3	3	3	3					
E3SM-1-1	3 incomplete scenarios	5.3	1				1					
EC-Earth3		4.3	73	7	30	7	58	5	5	5	5	5
EC-Earth3-AerChem	2 <3 historical runs		2			1						
EC-Earth3-Veg	4 same institution	4.3	8	7	8	6	6					
FGOALS-f3-L	1 No tmax/tmin	3	3	3	3	3	3					
FGOALS-g3	1 No tmax/tmin	2.9	6	4	4	5	4					
FIO-ESM-2-0	3 incomplete scenarios		3	3	3		3					
GFDL-CM4	3 incomplete scenarios	3.9	1		1		1					
GFDL-ESM4		2.7	3	1	3	1	1	3	1	3	1	1
GISS-E2-1-G	selected r*i1p3f1 variants	2.7	47	7	30	19	7	4	4	4	4	4
HadGEM3-GC31-LL	5 shared components (UKESM1)	5.6	5	1	4		4	4				
HadGEM3-GC31-MM	3 incomplete scenarios	5.4	4	1			4					
IITM-ESM	1 No tmax/tmin		1	1	1	1	1					
INM-CM4-8	2 <3 historical runs	1.8	1	1	1	1	1					
INM-CM5-0		1.9	9	1	1	5	1	9	1	1	5	1
IPSL-CM6A-LR		4.6	9	5	6	9	5	9	5	6	9	5
KACE-1-0-G	1 No tmax/tmin		3	3	3	3	3					
KIOST-ESM	2 <3 historical runs		1	1	1		1					
MCM-UA-1-0	1 No tmax/tmin		2	1	1	1	1					
MIROC-ES2L	4 same institution	2.7	3	3	3	3	3	3				
MIROC6		2.6	50	50	50	3	50	10	10	10	3	10
MPI-ESM-1-2-HAM	3 incomplete scenarios		3			2						
MPI-ESM1-2-HR		3	10	2	2	10	2	8	2	2	10	1
MPI-ESM1-2-LR	4 same institution	3	10	10	10	10	10	10				
MRI-ESM2-0		3.1	7	1	5	5	2	5	1	5	1	1
NESM3	5 shared components (MPI-ESM1)	4.8	5	2	2		2	5				
NorESM2-LM	1 No tmax/tmin	2.6	3	1	3	3	1					
NorESM2-MM	1 No tmax/tmin	2.5	1	1	2	1	1					
TaiESM1	1 No tmax/tmin	4.4	2	1	1	1	1					
UKESM1-0-LL		5.4	19	16	17	16	5	10	5	5	5	5

237
238

239 **Table 2: Institution and citation for each model in the 13-model ensemble.**

Model	Institutions	Citation
ACCESS-ESM1.5	Commonwealth Scientific and Industrial Research Organisation (Australia)	Ziehn et al. (2020)
BCC-CSM2	Beijing Climate Center (China)	Wu et al. (2019)
CanESM5	Canadian Centre for Climate Modelling and Analysis (Canada)	Swart et al. (2019)
CNRM-ESM2-1	CNRM (Centre National de Recherches Meteorologiques) and CERFACS (Centre Europeen de Recherche et de Formation Avancee en Calcul Scientifique) (France)	S��ferian et al. (2019)
EC-Earth3	EC-Earth Consortium (European Community)	D��scher et al. (2021)
GFDL-ESM4	National Oceanic and Atmospheric Administration, Geophysical Fluid Dynamics Laboratory (USA)	Dunne et al. (2020)
GISS-E2.1	Goddard Institute for Space Studies (USA)	Kelley et al. (2020)
INM-CM5.0	Institute for Numerical Mathematics (Russia)	Volodin et al. (2017)
IPSL-CM6A-LR	Institut Pierre Simon Laplace (France)	Boucher et al. (2020)
MIROC6	JAMSTEC (Japan Agency for Marine-Earth Science and Technology), AORI (Atmosphere and Ocean Research Institute), NIES (National Institute for Environmental Studies), and R-CCS (RIKEN Center for Computational Science) (Japan)	Tatebe et al. (2018)
MPI-ESM1.2-HR	Max Planck Institute for Meteorology (Germany)	M��ller et al. (2018)
MRI-ESM2.0	Meteorological Research Institute (Japan)	Yukimoto et al. (2019)
UKESM1	Met Office Hadley Centre and Natural Environment Research Council (UK)	Sellar et al. (2019)

240

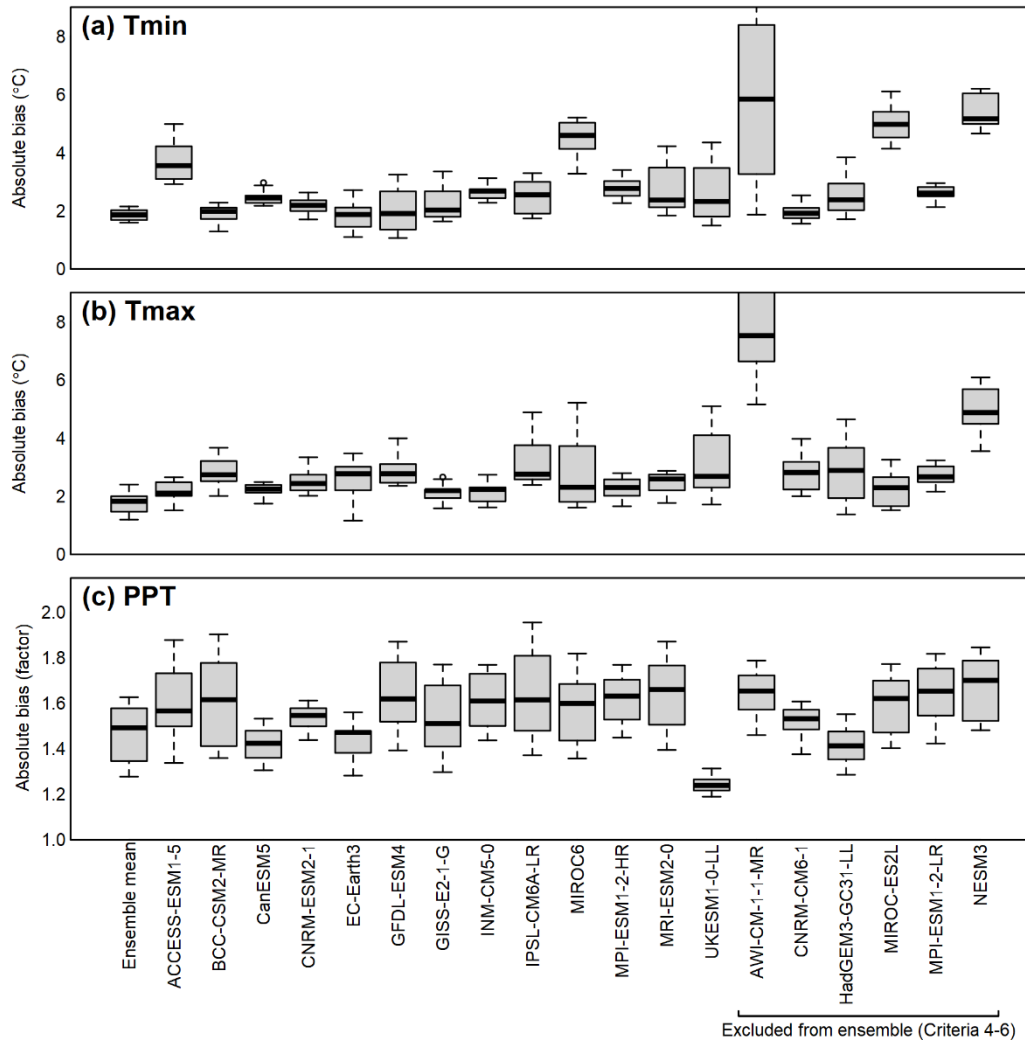
241 **3.2 Attributes of the 13-model ensemble**

242 **3.2.1 Representation of the full CMIP6 ensemble**

243 The 13-model ensemble has a mean global equilibrium climate sensitivity (ECS) of 3.7  C
 244 and a range of 1.9-5.6  C, which matches ECS of the full CMIP6 ensemble (3.7  C; 1.8-5.6  C)
 245 (Meehl et al. 2020).

246 **3.2.2 Model bias**

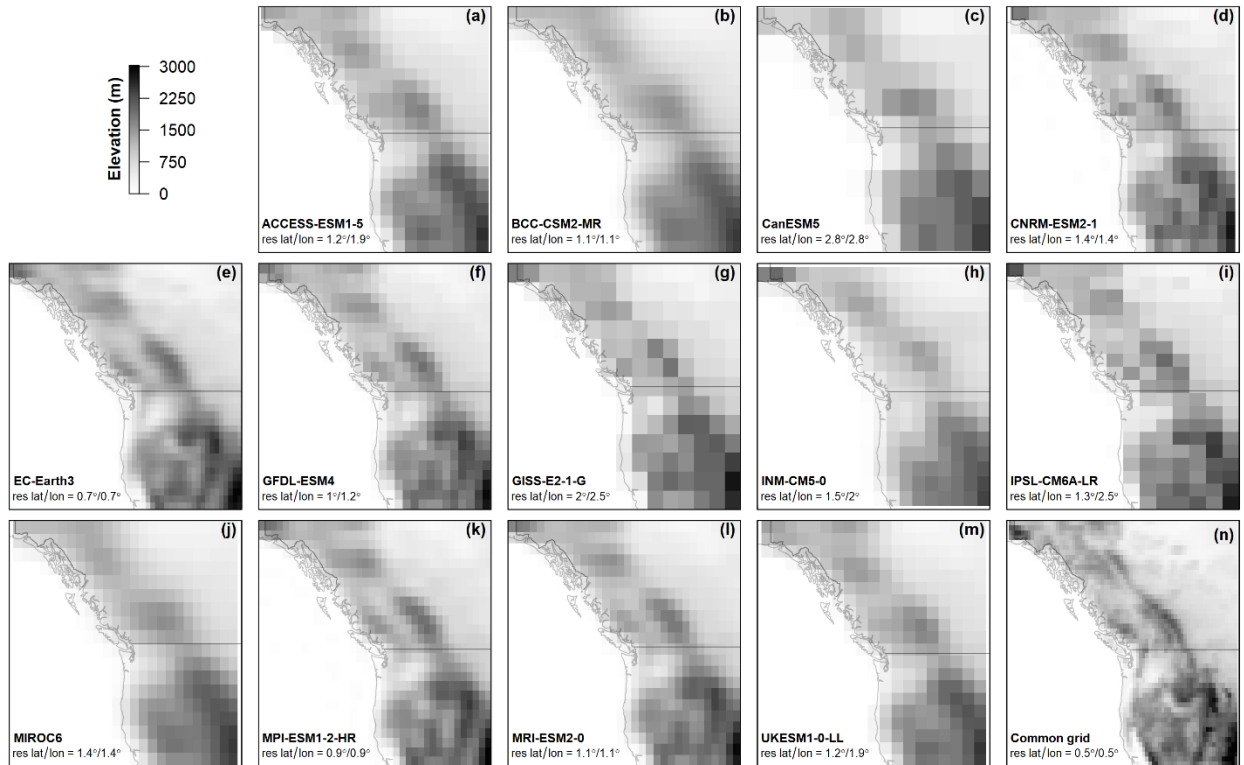
247 The ensemble mean has a mean absolute bias of 2  C in T_{\min} and T_{\max} . Most models have
 248 biases similar to this baseline. However, AWI-CM-1-1-MR has exceptionally high bias in both
 249 T_{\min} and T_{\max} . ACCESS-ESM1.5, MIROC6, MIROC-ES2L and NESM3 also have high biases in
 250 T_{\min} and/or T_{\max} . There is less differentiation in precipitation biases among models and with the
 251 ensemble mean. UKESM1, CanESM5, EC-Earth3, and HadGEM3-GC31 have lower
 252 precipitation biases than the ensemble mean.



253 **Figure 1: Model biases in monthly means of (a) daily minimum temperature, (b) daily maximum**
 254 **temperature, and (c) precipitation.** Each box represents 12 values of mean absolute bias over North
 255 America, one for each month. Absolute bias for precipitation is expressed as a factor of magnitude, e.g.,
 256 relative biases of 50% and 200% both have an absolute bias of 2.
 257

258 3.2.3 Spatial resolution and model orography

259 The selected 13-model ensemble has a mean latitudinal grid resolution of 1.4° (range of
 260 0.7° - 2.8°) (Figure 2). Four models (EC-Earth3, GFDL-ESM4, MPI-ESM1.2-HR, and MRI-
 261 ESM2.0) resolve the macrotopography of the Western Cordillera, namely the Sierra Nevada,
 262 Cascade Range, Rocky Mountains, and British Columbia Coast Ranges. BCC-CSM2-MR does
 263 not resolve these ranges, despite having sufficient grid resolution to do so. CanESM5 has a very
 264 low resolution of $2.8^\circ \times 2.8^\circ$.



265
 266 **Figure 2: Effective topographic resolution of the 13 selected models.** (a-m) model orography
 267 (elevation of land surface) in the native grid of each model. The extent of the map is central-western
 268 North America (106-142°W, 37-62°N). The common grid (panel n) is the 0.5° grid used for extraction of
 269 observations from ClimateNA.

270 3.2.4 Projected climate change

271 A visual comparison of projected seasonal changes in T_{\min} , T_{\max} , and PPT (Figure 3)
 272 indicates some basic attributes of the ensemble simulations. All models exhibit Arctic
 273 amplification of winter temperatures, though it is relatively subtle in EC-Earth3. Most models
 274 project the strongest summer warming at mid-latitudes. All models, with the exception of
 275 UKESM1, have a similar pattern of warming in T_{\min} and T_{\max} , though the magnitude of warming
 276 is greater for T_{\min} in most models.

277 Continental-scale patterns of winter (Dec-Feb) precipitation change are somewhat
 278 consistent among models, with declines in Mexico and increases in the Arctic regions.
 279 Deviations from this pattern are strongest in models with few (1-3) historical runs for SSP2-4.5
 280 (BCC-CSM2-MR, GFDL-ESM4 and INM-CM5.0), and are likely due to internal variability.
 281 This result indicates the benefit of multiple runs in smoothing out natural variability to reveal the
 282 anthropogenic climate change signal in noisy climate variables like precipitation and winter
 283 temperature.

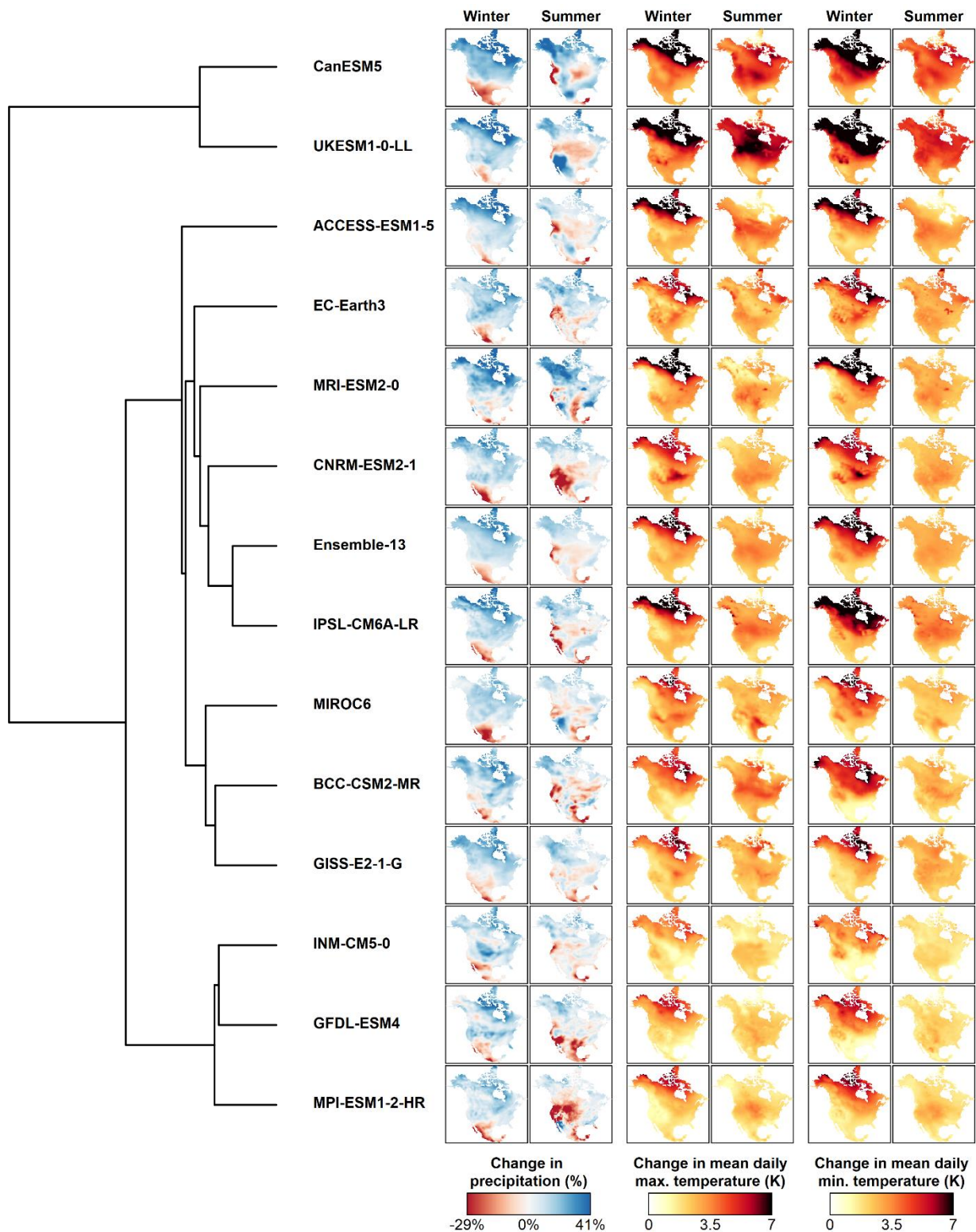
284 Most models project a reduction in summer (Jun-Aug) precipitation in the coastal areas of
 285 the Pacific Northwest (California, Oregon, Washington, and southern British Columbia). There
 286 is substantial disagreement among models in summer precipitation change over the rest of the
 287 continent. The muted summer precipitation change in the ensemble mean hides this ensemble

288 disagreement, and underscores the importance of assessing climate change impacts with an
289 ensemble of model projections rather than solely using the ensemble mean.

290 The two high-ECS models CanESM5 and UKESM1 have similar patterns and magnitudes
291 of change in winter temperature and precipitation. However, they differ substantially in the
292 summer, with UKESM1 showing much higher increases in daytime temperatures (T_{\max}) in
293 Temperate and Boreal regions and stronger declines in precipitation in Central North America.
294 Although CanESM5 has a higher ECS and stronger trend in 1970-2014 global heating (Liang et
295 al. 2020), UKESM1 projects stronger mid-century heating over North America.

296

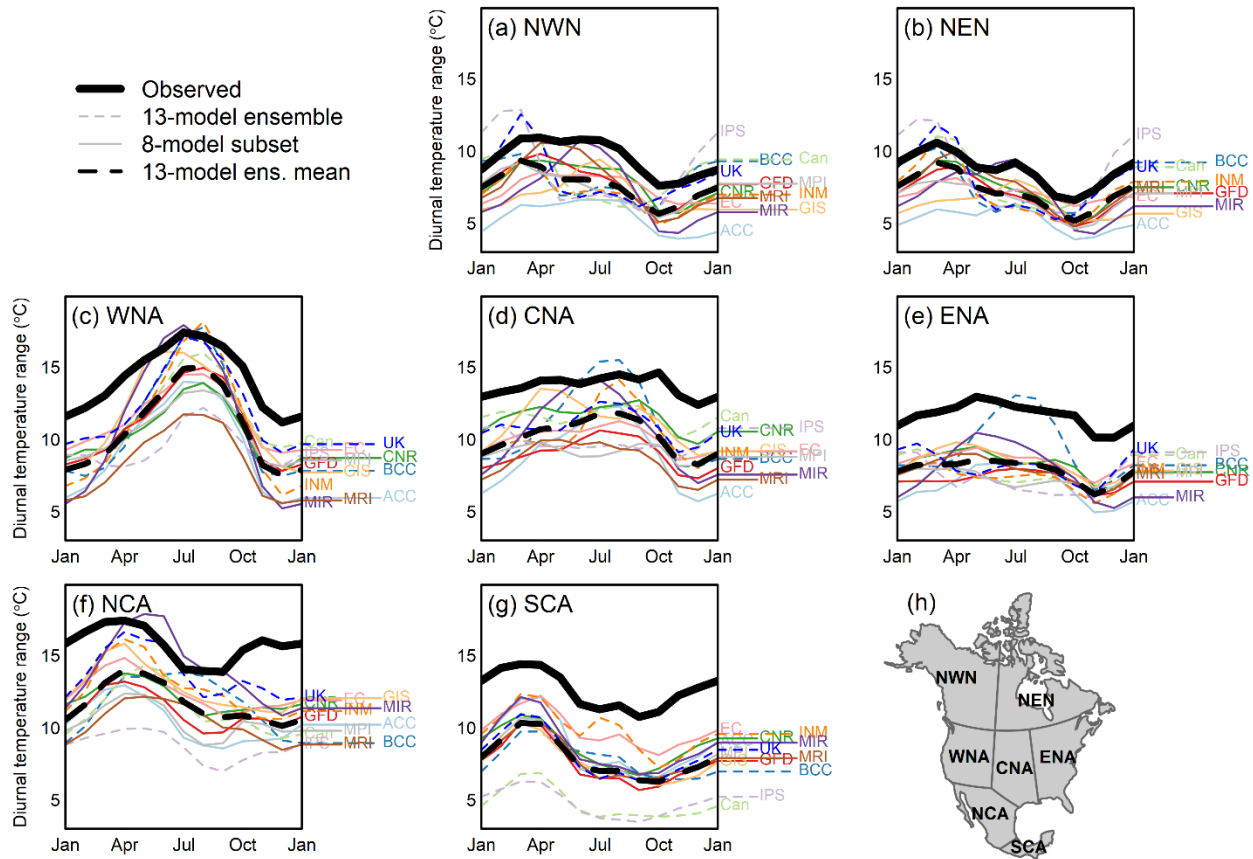
297



298 **Figure 3: Spatial variation in climate change responses among the 13-model ensemble.** Mapped
 299 climate changes are for the mean projected climate of the 2041-2060 period (SSP2-4.5). Precipitation is
 300 log-scaled to provide proportional magnitude of positive and negative changes. Models are structured by
 301 a cluster dendrogram of spatial similarity in seasonal climate changes in all three climate elements.

302 3.2.5 Diurnal temperature range

303 The models consistently underestimate the diurnal temperature range (DTR), measured as
 304 the difference between T_{min} and T_{max} (Figure 4). However, the 13-model ensemble and the 8-
 305 model subset (described in Section 3.3) reproduce the observed seasonal cycle in all regions.
 306 Models that deviate most from the ensemble mean seasonal cycle generally are those excluded
 307 from the 8-model subset, namely IPSL-CM6A-LR (high amplitude in Arctic regions and
 308 underestimated elsewhere), BCC-CSM2-MR (high amplitude at midlatitudes), and UKESM1-0-
 309 LL (high amplitude in Arctic regions and WNA). Among the 8-model subset, MIROC6
 310 overestimates the amplitude of the seasonal cycle in most regions.

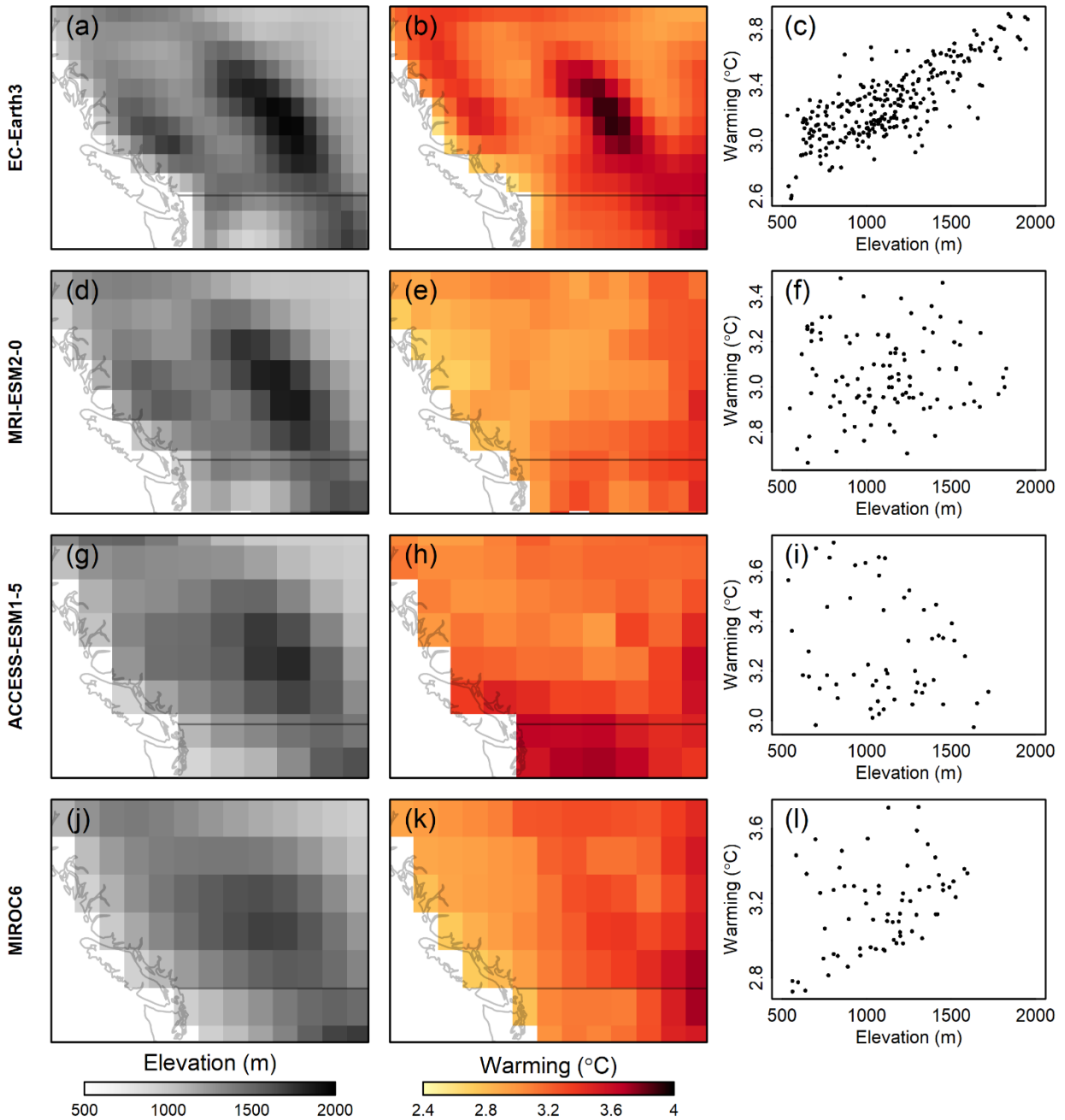


311 **Figure 4: Seasonal cycle of the mean diurnal temperature range in observations and the 13-model**
 312 **ensemble, averaged over each IPCC reference region (h, Iturbide et al. 2020).** Mean diurnal
 313 temperature range is calculated as the difference between monthly 1961-1990 normals of T_{min} and
 314 T_{max}. Observations are the ClimateNA composite of PRISM and WorldClim gridded climate normals.
 315 Model abbreviations are the first 2-3 letters of the model name.
 316

317 3.2.6 Elevation-dependent warming

318 There are large differences among models in the representation of elevation-dependent warming.
 319 These differences are demonstrated using a subset of the ensemble over the Coast Range and
 320 Rocky Mountains of southwestern Canada (Figure 5). EC-Earth3 and MRI-ESM2.0 both resolve
 321 these mountain ranges in their model orography (Figure 5a,d). EC-Earth3 has a strong signal of
 322 elevation-dependent warming, in which the Rocky Mountains warm ~0.8°C (25%) more than the

323 adjacent plateaus (Figure 5b,c). In contrast, MRI-ESM2.0 exhibits no relationship between
 324 elevation and warming (Figure 5e,f). ACCESS-ESM1.5 and MIROC6 represent the mountain
 325 ranges as a single feature in their model orography. ACCESS-ESM1.5 exhibits a weak negative
 326 relationship of warming to elevation, and MIROC6 exhibits a weak positive relationship.

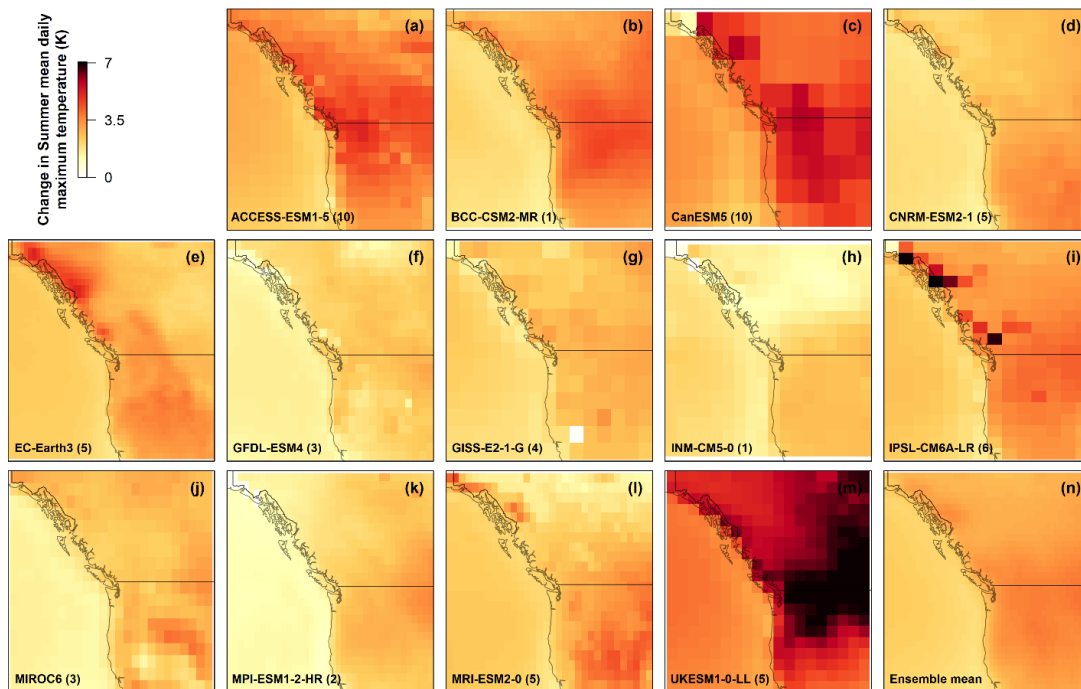


327
 328 **Figure 5: Relationships between elevation and warming (autumn Tmax) over southwestern Canada**
 329 **in four CMIP6 models.** To emphasize spatial variation within each model rather than warming
 330 magnitude among models, warming for each model is selected from different periods: 2041-2060 for EC-
 331 Earth3 and ACCESS-ESM1.5; 2061-2080 for MRI-ESM2.0; and 2081-2100 for MIROC6. Projected
 332 warming is under SSP2-4.5 for all models. Coastal cells (elevation <500m) are excluded to reduce the
 333 maritime influence on the analysis.

334 **3.3 Ensemble subset selection**

335 **3.3.1 Screening exclusions**

336 The following models are prioritized for exclusion from subsets of the ensemble based on
337 combinations of the four screening criteria: **CanESM5**, because its very high climate sensitivity
338 (ECS 5.6°C) is also represented by UKESM1.0-LL and because its very low horizontal
339 resolution is less suitable for downscaling; **INM-CM5.0**, because it has very low climate
340 sensitivity (ECS 1.9°C) and is an outlier among CMIP6 models for under-representing the
341 observed 1975-2014 global temperature trend (Liang et al. 2020) (Criterion 7). In addition, this
342 model has only one simulation for most scenarios, producing a less robust climate signal
343 (Criterion 9); **BCC-CSM2-MR**, due to having a single simulation for each scenario (Criterion 9)
344 and low topographic resolution (Criterion 8); and **IPSL-CM6A-LR**, due to isolated grid cells
345 with very high summer warming in the BC Coast Ranges and Southeast Alaska (Figure 6;
346 Criterion 10). The warming in these cells may be physically plausible in the model's simplified
347 topography, but is problematic for downscaling to higher spatial resolutions.



348 **Figure 6: Summer daytime warming in the 13-model ensemble over central-western North America**
349 **(106-142W, 37-62N).** Values are the change in summer T_{\max} for the 2041-2060 period (SSP2-4.5),
350 relative to 1961-1990, in the native model grid. Change is calculated from the mean of multiple
351 simulation runs per model, specified next to the model name.
352

353 UKESM1 also has very high climate sensitivity, similar to CanESM5, that is assessed as
354 very unlikely based on observational evidence (Sherwood et al. 2020, Arias et al. 2021). Some
355 researchers may wish to constrain their ensemble subset to observations by excluding this model.
356 Others may wish to include a high-sensitivity model in their subset as a representation of the
357 long tail of uncertainty in the upper limit of climate sensitivity (Sutton 2018). To accommodate
358 both perspectives, we provide structured subsets with and without UKESM1 in the ordered
359 ensemble subsets. We preferred UKESM1 over CanESM5 as a representative of high-sensitivity

360 models due to its higher grid resolution and closer alignment with the observed post-1970 global
 361 heating trend (Liang et al. 2020).

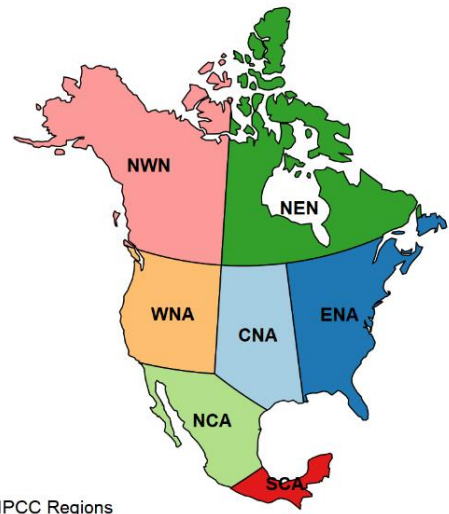
362 The 8-model subset has a mean global ECS of 3.4°C (2.6-4.8°C). The 9-model subset that
 363 includes UKESM1 has a mean global ECS of 3.6°C (2.6-5.4°C), using ECS values provided by
 364 Meehl et al. (2020).

365 **3.3.2 Ordered subsets**

366 Table 3 specifies ordered subsets of the models that passed screening criteria 7-10. For a
 367 desired region and subset size, the ensemble subset for each region includes all models listed at
 368 and above the desired subset size. For example, a 4-model ensemble for the NEN region would
 369 include CNRM-ESM2-1, UKESM1.0-LL, EC-Earth3, and MPI-ESM1.2-HR. The considerable
 370 variation among regions in the order of the subsets underscores the spatial variation in climate
 371 change responses across North America. The exception to this variation in model order is that
 372 UKESM1 is the second model in all regions. Since the first position in the order is the model
 373 closest to the ensemble centroid and the second position is the model furthest from the centroid,
 374 this result indicates that UKESM1 consistently projects the most extreme climate changes
 375 throughout the continent.

Table 3: Ordered subsets of the 13-model ensemble. Subsets are provided for North America (NAM) and the 7 IPCC reference regions (Figure 7). Model abbreviations are ACC (ACCESS-ESM1.5), CNRM (CNRM-ESM2-1), EC (EC-Earth3), GFDL (GFDL-ESM4), GISS (GISS-E2-1-G), MIR (MIROC6), MPI (MPI-ESM1.2-HR), MRI (MRI-ESM2.0), and UK (UKESM1.0-LL). Exclusion of UKESM1 provides an ensemble that is consistent with assessed constraints on equilibrium climate sensitivity.

Subset size	IPCC Reference Region							
	NEN	NWN	WNA	CNA	ENA	NCA	SCA	NAM
Including UKESM1-0-LL								
1	CNRM	CNRM	MRI	ACC	EC	MRI	MRI	CNRM
2	UK	UK	UK	UK	UK	UK	UK	UK
3	EC	MPI	MPI	MPI	MPI	GFDL	GFDL	MPI
4	MPI	EC	GISS	CNRM	MRI	MIR	MIR	MRI
5	MRI	ACC	MIR	MIR	MIR	EC	EC	EC
6	ACC	MRI	CNRM	GISS	GFDL	MPI	MPI	MIR
7	GFDL	MIR	GFDL	EC	ACC	CNRM	CNRM	ACC
8	GISS	GISS	EC	GFDL	GISS	ACC	ACC	GISS
9	MIR	GFDL	ACC	MRI	CNRM	GISS	GISS	GFDL
Excluding UKESM1-0-LL								
1	CNRM	CNRM	MRI	MRI	GISS	GISS	GISS	CNRM
2	EC	EC	MPI	MPI	GFDL	EC	EC	MPI
3	MPI	ACC	GISS	CNRM	MRI	MRI	MRI	EC
4	MRI	MPI	MIR	MIR	ACC	MIR	MIR	MRI
5	ACC	MIR	CNRM	EC	CNRM	GFDL	GFDL	ACC
6	GISS	GISS	EC	GFDL	EC	CNRM	CNRM	GISS
7	GFDL	MRI	GFDL	GISS	MPI	ACC	ACC	MIR
8	MIR	GFDL	ACC	ACC	MIR	MPI	MPI	GFDL



IPCC Regions
Figure 7: IPCC reference regions (Iturbide et al. 2020) used for ordered subsets of the ensemble.

376 4 Discussion

377 We selected 13 CMIP6 models from a candidate pool of 44 models contributing to the
378 CMIP6 experiment. This 13-model ensemble is representative of the distribution of equilibrium
379 climate sensitivity in the full CMIP6 ensemble. The 13-model ensemble facilitates robust
380 downscaling by using multiple simulations per scenario for each model and excluding models
381 with high bias. We provided rationale for an 8-member subset of the ensemble based on
382 screening criteria and order these 8 models for selection of smaller ensembles for regional
383 analysis in North America. We also highlighted some tradeoffs among the models in terms of
384 grid resolution, number of simulation runs, climate sensitivity, regional biases, and local
385 artefacts. These results, and the accompanying web application ([https://bcgov-
386 env.shinyapps.io/cmip6-NA/](https://bcgov-env.shinyapps.io/cmip6-NA/)), help readers to make model selections appropriate to their specific
387 research objectives.

388 4.1 Model bias

389 The bias assessment was a useful way to identify models with extreme divergence from the
390 observed climate. High biases were the sole basis for the exclusion of one model, AWI-CM1-1-
391 1-MR, and are an attribute of concern in two of the models selected for the ensemble, ACCESS-
392 ESM1.5 and MIROC6. The moderate biases in the rest of the ensemble, however, do not
393 necessarily indicate a problem with the models. Bias is the difference between model
394 simulations and the observed climate. We controlled the confounding influence of natural
395 variability in each model by calculating bias using the mean of several simulation runs. This
396 measure is not possible for observations since there is only one realization of the observed
397 climate. Natural variability in the observed climate, therefore, could produce apparent biases
398 even in a hypothetical “perfect” model (Lanzante et al. 2018). The ensemble mean absolute bias
399 of 2°C in temperature and by a factor of 1.5 in precipitation cannot be definitively attributed to
400 the models or the ensemble; it is to some extent an artefact of natural variability in the observed
401 climate.

402 4.2 Grid resolution

403 Four of the models in the ensemble have horizontal grid resolution sufficient to resolve
404 major mountain ranges. One model (EC-Earth3) has relatively high resolution (0.7°x0.7°)
405 approaching the previous generation of regional climate models used for dynamical downscaling.
406 The trend towards higher resolution is encouraging, but the benefits of moderate resolution
407 models for km-scale downscaling are ambiguous. On one hand, resolving mountain ranges
408 allows for stronger differentiation of maritime/continental transitions (Lanzante et al. 2018),
409 windward and leeward dynamics (Kanehama et al. 2019), and elevation-dependent climate
410 changes (Palazzi et al. 2019). On the other hand, these resolved mountain ranges are still highly
411 simplified features in even the highest resolution models in the ensemble. Resolved high-
412 elevation processes such as enhanced warming due to snow albedo feedbacks (Salathé et al.
413 2008) will be applied to unresolved low-elevation locations (e.g., valleys) during change-factor
414 downscaling. Hence, higher-resolution models offer new insights, but also introduce new
415 problems for statistical downscaling. In the absence of additional downscaling measures to
416 address these problems, we do not view the higher-resolution models in the ensemble as

417 intrinsically more valuable or valid. They do, however, make a distinct contribution and the
418 range of grid resolution in the ensemble improves the representation of modeling uncertainties.

419 **4.3 Diurnal temperature range**

420 Underestimation of DTR is a persistent feature of climate models (Wang and Clow 2020).
421 Intermodel differences in DTR can be attributed to differences in parameterizations for clouds,
422 aerosols and soil moisture, among others (Lindvall and Svensson 2015). However, the consistent
423 underestimation of DTR relative to observations has not been definitively explained. Part of the
424 underestimation of DTR may be due to differences in the timescale of DTR measurement in
425 observations and models; since T_{\min} and T_{\max} are measured instantaneously in observations but
426 simulated over longer timesteps in models, models are expected to have lower DTR (Wilson et
427 al. 2008, Rupp et al. 2013). To the extent that underestimation of DTR is an artefact of the
428 different timescales of measurement in observations and models, rather than of systematic biases
429 in the driving processes, some overestimation of T_{\min} and underestimation of T_{\max} can be
430 expected even from a perfect model.

431 **4.4 Reconciling the equilibrium climate sensitivity of the ensemble with observational** 432 **constraints**

433 The 13-model ensemble selected here, like the full CMIP6 ensemble, has a mean (3.7 °C)
434 and upper limit (5.6°C) of equilibrium climate sensitivity that substantially exceeds the IPCC
435 AR6 assessed best estimate ECS of 3°C and *very likely* upper limit of 5°C (Arias et al. 2021). In
436 other words, the 13-model ensemble contains models that simulate stronger global warming than
437 is supported by multiple lines of observational evidence. Five (38%) of the 13 models are above
438 the IPCC AR6 assessed *likely* upper limit on ECS of 4 °C, and two (15%) of the models are
439 above the *very likely* upper limit of 5°C. If the ensemble were to strictly conform to the IPCC
440 assessed range, there would be only two models exceeding 4 °C ECS and no models exceeding
441 5°C, following the IPCC’s probabilistic definitions of *likely* (one-sided $p>83\%$) and *very likely*
442 (one-sided $p>95\%$).

443 The need to reconcile the CMIP ensemble ECS range with observational constraints is a
444 new dilemma for climate change impacts and adaptation researchers. It is long been agreed that
445 model democracy (one model, one vote) is not a strictly valid method of assessing climate
446 change uncertainty (Knutti 2010, Leduc et al. 2016). However, in the past this objection was
447 somewhat academic since the distribution of ECS in CMIP ensembles approximately matched
448 the (wider) range of ECS supported by other lines of evidence. For practical purposes it was
449 reasonable for analysts to use the multimodel ensemble spread in previous CMIP generations as
450 a proxy for scientific uncertainty on climate change. This approach is no longer valid given the
451 incongruence between the CMIP6 ensemble range of ECS and the IPCC assessed range. Careful
452 model selection is now required to avoid biasing regional climate change analyses.

453 There are several viable approaches to constrain CMIP6 ensembles in downscaled regional
454 analyses. Weighting the models based on observational constraints is possible for regional
455 analyses (Ribes et al. 2021). However, in practice many analyses will require simply selecting a
456 subset of the CMIP6 ensemble that is closer to the IPCC assessed range, as we have done with
457 the 8-model subset. The disadvantage of this approach is that it discards valuable information

458 from the excluded models. The CanESM5 and UKESM1 models are advanced models from
459 highly respected modeling centers, with demonstrated skill in modeling many Earth system
460 processes (Eyring et al. 2021). Further, these models have large ensembles of simulations for
461 each scenario (50 runs, in the case of CanESM5) which are useful for quantifying natural
462 variability. Expressing variables of interest relative to the amount of regional or global warming
463 is a widely practiced technique that facilitates inclusion of high-ECS models by removing the
464 timing of the warming as a factor in the ensemble spread. It is conceivable that both techniques
465 could be used in a single study; to use the 8-model ensemble for time-relevant analyses and a
466 larger ensemble for analyses where the warming level is more relevant. These considerations
467 highlight that the full CMIP6 ensemble is a somewhat arbitrary collection of non-independent
468 models, and careful ensemble selection is necessary to achieve a meaningful representation of
469 modeling uncertainty.

470 **5 Data Availability**

471 Downscaled projections for the selected 13 CMIP6 models are available in ClimateNA
472 (<http://climatena.ca/>), which provides downscaling at user-specified spatial resolution and
473 various temporal intervals (annual, 20-year and 30-year periods). An accompanying web
474 application (<https://bcgov-env.shinyapps.io/cmip6-NA/>) provides tools for model selection and
475 visualization of the ensemble.

476 **6 Acknowledgements**

477 We acknowledge the World Climate Research Programme, which, through its Working
478 Group on Coupled Modelling, coordinated and promoted CMIP6. We thank the climate
479 modeling groups for producing and making available their model output, the Earth System Grid
480 Federation (ESGF) for archiving the data and providing access, and the multiple funding
481 agencies who support CMIP6 and ESGF.

482

483 **7 Literature Cited**

484 Arias, P. A., N. Bellouin, E. Coppola, R. G. Jones, G. Krinner, J. Marotzke, V. Naik, M. D.
 485 Palmer, J. G-K. Plattner, Rogelj, M. Rojas, J. Sillmann, T. Storelvmo, P. W. Thorne, B.
 486 Trewin, K. A. Rao, B. Adhikary, R. P. Allan, K. Armour, G. Bala, R. Barimalala, S. Berger,
 487 J. G. Canadell, C. Cassou, A. Cherchi, W. Collins, W. D. Collins, S. L. Connors, S. Corti, F.
 488 Cruz, F. J. Dentener, C. Dereczynski, A. Di Luca, A. D. Niang, F. J. Doblas-Reyes, A.
 489 Dosio, H. Douville, F. Engelbrecht, V. Eyring, E. Fischer, P. Forster, B. Fox-Kemper, J. S.
 490 Fuglestvedt, J. C. Fyfe, N. P. Gillett, L. Goldfarb, I. Gorodetskaya, J. M. Gutierrez, R.
 491 Hamdi, E. Hawkins, H. T. Hewitt, P. Hope, A. S. Islam, C. Jones, D. S. Kaufman, R. E.
 492 Kopp, Y. Kosaka, J. Kossin, S. Krakovska, J.-Y. Lee, J. Li, T. Mauritsen, T. K. Maycock,
 493 M. Meinshausen, S.-K. Min, P. M. S. Monteiro, T. Ngo-Duc, F. Otto, I. Pinto, A. Pirani, K.
 494 Raghavan, R. Ranasinghe, A. C. Ruane, L. Ruiz, J.-B. Sallée, B. H. Samset, S.
 495 Sathyendranath, S. I. Seneviratne, A. A. Sörensson, S. Szopa, I. Takayabu, A.-M. Treguier,
 496 B. van den Hurk, R. Vautard, S. Z. K. von Schuckmann, X. Zhang, and K. Zickfeld. 2021.
 497 Technical Summary. Pages TS1-150 in V. Masson-Delmotte, P. Zhai, A. Pirani, S. L.
 498 Connors, C. Péan, S. Berger, N. Caud, Y. Chen, L. Goldfarb, M. I. Gomis, M. Huang, K.
 499 Leitzell, E. Lonnoy, J. B. R. Matthews, T. K. Maycock, T. Waterfield, O. Yelekçi, R. Yu,
 500 and B. Zhou, editors. *Climate Change 2021: The Physical Science Basis. Contribution of*
 501 *Working Group I to the Sixth Assessment Report of the Intergovernmental Panel on*
 502 *Climate Change.* Cambridge University Press.

503 Boucher, O., J. Servonnat, A. L. Albright, O. Aumont, Y. Balkanski, V. Bastrikov, S. Bekki, R.
 504 Bonnet, S. Bony, L. Bopp, P. Braconnot, P. Brockmann, P. Cadule, A. Caubel, F. Cheruy,
 505 F. Codron, A. Cozic, D. Cugnet, F. D'Andrea, P. Davini, C. de Lavergne, S. Denvil, J.
 506 Deshayes, M. Devilliers, A. Ducharne, J. L. Dufresne, E. Dupont, C. Éthé, L. Fairhead, L.
 507 Falletti, S. Flavoni, M. A. Foujols, S. Gardoll, G. Gastineau, J. Ghattas, J. Y. Grandpeix, B.
 508 Guenet, L. E. Guez, E. Guilyardi, M. Guimberteau, D. Hauglustaine, F. Hourdin, A.
 509 Idelkadi, S. Joussaume, M. Kageyama, M. Khodri, G. Krinner, N. Lebas, G. Levavasseur,
 510 C. Lévy, L. Li, F. Lott, T. Lurton, S. Luyssaert, G. Madec, J. B. Madeleine, F. Maignan, M.
 511 Marchand, O. Marti, L. Mellul, Y. Meurdesoif, J. Mignot, I. Musat, C. Ottlé, P. Peylin, Y.
 512 Planton, J. Polcher, C. Rio, N. Rochetin, C. Rousset, P. Sepulchre, A. Sima, D.
 513 Swingedouw, R. Thiéblemont, A. K. Traore, M. Vancoppenolle, J. Vial, J. Vialard, N.
 514 Viovy, and N. Vuichard. 2020. Presentation and Evaluation of the IPSL-CM6A-LR Climate
 515 Model. *Journal of Advances in Modeling Earth Systems* 12:1–52.

516 Brunner, L., R. Lorenz, M. Zumwald, and R. Knutti. 2019. Quantifying uncertainty in European
 517 climate projections using combined performance-independence weighting. *Environmental*
 518 *Research Letters* 14:124010.

519 Cannon, A. J. 2015. Selecting GCM scenarios that span the range of changes in a multimodel
 520 ensemble: Application to CMIP5 climate extremes indices. *Journal of Climate* 28:1260–
 521 1267.

522 Cannon, A. J. 2018. Multivariate quantile mapping bias correction: an N-dimensional probability
 523 density function transform for climate model simulations of multiple variables. *Climate*
 524 *Dynamics* 50:31–49.

- 525 Döscher, R., M. Acosta, A. Alessandri, P. Anthoni, A. Arneth, T. Arsouze, T. Bergmann, R.
526 Bernadello, S. Bousetta, L.-P. Caron, G. Carver, M. Castrillo, F. Catalano, I. Cvijanovic, P.
527 Davini, E. Dekker, F. Doblas-Reyes, D. Docquier, P. Echevarria, U. Fladrich, R. Fuentes-
528 Franco, M. Gröger, J. v. Hardenberg, J. Hieronymus, M. P. Karami, J.-P. Keskinen, T.
529 Koenigk, R. Makkonen, F. Massonnet, M. Ménégos, P. Miller, E. Moreno-Chamarro, L.
530 Nieradzic, T. van Noije, P. Nolan, D. O'Donnell, P. Ollinaho, G. van den Oord, P. Ortega,
531 O. T. Prims, A. Ramos, T. Reerink, C. Rousset, Y. Ruprich-Robert, P. Le Sager, T.
532 Schmith, R. Schrödner, F. Serva, V. Sicardi, M. Sloth Madsen, B. Smith, T. Tian, E.
533 Tourigny, P. Uotila, M. Vancoppenolle, S. Wang, D. Wårlind, U. Willén, K. Wyser, S.
534 Yang, X. Yepes-Arbós, and Q. Zhang. 2021. The EC-Earth3 Earth System Model for the
535 Climate Model Intercomparison Project 6. Geoscientific Model Development Discussions
536 Preprint:1–90.
- 537 Dunne, J. P., L. W. Horowitz, A. J. Adcroft, P. Ginoux, I. M. Held, J. G. John, J. P. Krasting, S.
538 Malyshev, V. Naik, F. Paulot, E. Shevliakova, C. A. Stock, N. Zadeh, V. Balaji, C. Blanton,
539 K. A. Dunne, C. Dupuis, J. Durachta, R. Dussin, P. P. G. Gauthier, S. M. Griffies, H. Guo,
540 R. W. Hallberg, M. Harrison, J. He, W. Hurlin, C. McHugh, R. Menzel, P. C. D. Milly, S.
541 Nikonov, D. J. Paynter, J. Ploshay, A. Radhakrishnan, K. Rand, B. G. Reichl, T. Robinson,
542 D. M. Schwarzkopf, L. T. Sentman, S. Underwood, H. Vahlenkamp, M. Winton, A. T.
543 Wittenberg, B. Wyman, Y. Zeng, and M. Zhao. 2020. The GFDL Earth System Model
544 Version 4.1 (GFDL-ESM 4.1): Overall Coupled Model Description and Simulation
545 Characteristics. *Journal of Advances in Modeling Earth Systems* 12:e2019MS002015.
- 546 Eyring, V., S. Bony, G. A. Meehl, C. A. Senior, B. Stevens, R. J. Stouffer, and K. E. Taylor.
547 2016. Overview of the Coupled Model Intercomparison Project Phase 6 (CMIP6)
548 experimental design and organization. *Geoscientific Model Development* 9:1937–1958.
- 549 Eyring, V., N. P. Gillett, K. M. A. Rao, R. Barimalala, M. B. Parrillo, N. Bellouin, C. Cassou, P.
550 J. Durack, Y. Kosaka, S. McGregor, S. Min, O. Morgenstern, and Y. Sun. 2021. Human
551 influence on the climate system. Pages 1–202 *in* V. Masson-Delmotte, P. Zhai, A. Pirani, S.
552 L. Connors, C. Péan, S. Berger, N. Caud, Y. Chen, L. Goldfarb, M. I. Gomis, M. Huang, K.
553 Leitzell, E. Lonnoy, J. B. R. Matthews, T. K. Maycock, T. Waterfield, O. Yelekçi, R. Yu,
554 and B. Zhou, editors. *Climate Change 2021: The Physical Science Basis. Contribution of*
555 *Working Group I to the Sixth Assessment Report of the Intergovernmental Panel on*
556 *Climate Change*. Cambridge University Press.
- 557 Fick, S. E., and R. J. Hijmans. 2017. WorldClim 2: new 1-km spatial resolution climate surfaces
558 for global land areas. *International Journal of Climatology* 37:4302–4315.
- 559 Hamann, A., T. Wang, D. L. Spittlehouse, and T. Q. Murdock. 2013. A comprehensive, high-
560 resolution database of historical and projected climate surfaces for western North America.
561 *Bulletin of the American Meteorological Society* 94:1307–1309.
- 562 Hijmans, R. J., S. E. Cameron, J. L. Parra, P. G. Jones, and A. Jarvis. 2005. Very high resolution
563 interpolated climate surfaces for global land areas. *International Journal of Climatology*
564 25:1965–1978.

- 565 Hui, Y., Y. Xu, J. Chen, C. Y. Xu, and H. Chen. 2020. Impacts of bias nonstationarity of climate
566 model outputs on hydrological simulations. *Hydrology Research* 51:925–941.
- 567 Hunter, R. D., and R. K. Meentemeyer. 2005. Climatologically aided mapping of daily
568 precipitation and temperature. *Journal of Applied Meteorology* 44:1501–1510.
- 569 Iturbide, M., J. M. Gutiérrez, L. M. Alves, J. Bedia, R. Cerezo-Mota, E. Gimadevilla, A. S.
570 Cofiño, A. Di Luca, S. H. Faria, I. V. Gorodetskaya, M. Hauser, S. Herrera, K. Hennessy,
571 H. T. Hewitt, R. G. Jones, S. Krakovska, R. Manzanás, D. Martínez-Castro, G. T. Narisma,
572 I. S. Nurhati, I. Pinto, S. I. Seneviratne, B. van den Hurk, and C. S. Vera. 2020. An update
573 of IPCC climate reference regions for subcontinental analysis of climate model data:
574 definition and aggregated datasets. *Earth System Science Data* 12:2959–2970.
- 575 Kanehama, T., I. Sandu, A. Beljaars, A. van Niekerk, and F. Lott. 2019. Which Orographic
576 Scales Matter Most for Medium-Range Forecast Skill in the Northern Hemisphere Winter?
577 *Journal of Advances in Modeling Earth Systems* 11:3893–3910.
- 578 Kelley, M., G. A. Schmidt, L. S. Nazarenko, S. E. Bauer, R. Ruedy, G. L. Russell, A. S.
579 Ackerman, I. Aleinov, M. Bauer, R. Bleck, V. Canuto, G. Cesana, Y. Cheng, T. L. Clune,
580 B. I. Cook, C. A. Cruz, A. D. Del Genio, G. S. Elsaesser, G. Faluvegi, N. Y. Kiang, D. Kim,
581 A. A. Lacis, A. Leboissetier, A. N. LeGrande, K. K. Lo, J. Marshall, E. E. Matthews, S.
582 McDermid, K. Mezuman, R. L. Miller, L. T. Murray, V. Oinas, C. Orbe, C. P. García-
583 Pando, J. P. Perlwitz, M. J. Puma, D. Rind, A. Romanou, D. T. Shindell, S. Sun, N.
584 Tausnev, K. Tsigaridis, G. Tselioudis, E. Weng, J. Wu, and M. S. Yao. 2020. GISS-E2.1:
585 Configurations and Climatology. *Journal of Advances in Modeling Earth Systems*
586 12:e2019MS002025.
- 587 Knutti, R. 2010. The end of model democracy? *Climatic Change* 102:395–404.
- 588 Lanzante, J. R., K. W. Dixon, M. J. Nath, C. E. Whitlock, and D. Adams-Smith. 2018. Some
589 pitfalls in statistical downscaling of future climate. *Bulletin of the American Meteorological*
590 *Society* 99:791–803.
- 591 Leduc, M., R. Laprise, R. de Elia, and L. Separovic. 2016. Is Institutional Democracy a Good
592 Proxy for Model Independence? *Journal of Climate* 29:8301–8316.
- 593 Lee, J. Y., J. Marotzke, G. Bala, L. Cao, S. Corti, J. P. Dunne, F. Engelbrecht, E. Fischer, J. C.
594 Fyfe, C. Jones, A. Maycock, J. Mutemi, O. Ndiaye, S. Panickal, and T. Zhou. 2021. Future
595 Global Climate: Scenario-Based Projections and Near-Term Information. Pages 4-1-4–195
596 in V. Masson-Delmotte, P. Zhai, A. Pirani, S. L. Connors, C. Péan, S. Berger, N. Caud, Y.
597 Chen, L. Goldfarb, M. I. Gomis, M. Huang, K. Leitzell, E. Lonnoy, J. B. R. Matthews, T.
598 K. Maycock, T. Waterfield, O. Yelekçi, R. Yu, and B. Zhou, editors. *Climate Change 2021:*
599 *The Physical Science Basis. Contribution of Working Group I to the Sixth Assessment*
600 *Report of the Intergovernmental Panel on Climate Change.* Cambridge University Press.
- 601 Liang, Y., N. P. Gillett, and A. H. Monahan. 2020. Climate Model Projections of 21st Century
602 Global Warming Constrained Using the Observed Warming Trend. *Geophysical Research*
603 *Letters* 47:1–10.

- 604 Lindvall, J., and G. Svensson. 2015. The diurnal temperature range in the CMIP5 models.
605 *Climate Dynamics* 44:405–421.
- 606 Maraun, D. 2016. Bias Correcting Climate Change Simulations - a Critical Review. *Current*
607 *Climate Change Reports* 2:211–220.
- 608 McSweeney, C. F., R. G. Jones, R. W. Lee, and D. P. Rowell. 2014. Selecting CMIP5 GCMs for
609 downscaling over multiple regions. *Climate Dynamics* 44:3237–3260.
- 610 Meehl, G. A., C. A. Senior, V. Eyring, G. Flato, J. F. Lamarque, R. J. Stouffer, K. E. Taylor, and
611 M. Schlund. 2020. Context for interpreting equilibrium climate sensitivity and transient
612 climate response from the CMIP6 Earth system models. *Science Advances* 6:1–11.
- 613 Milinski, S., N. Maher, and D. Olonscheck. 2019. How large does a large ensemble need to be?
614 *Earth System Dynamics Discussions*:1–19.
- 615 Müller, W. A., J. H. Jungclaus, T. Mauritsen, J. Baehr, M. Bittner, R. Budich, F. Bunzel, M.
616 Esch, R. Ghosh, H. Haak, T. Ilyina, T. Kleine, L. Kornblueh, H. Li, K. Modali, D. Notz, H.
617 Pohlmann, E. Roeckner, I. Stemmler, F. Tian, and J. Marotzke. 2018. A Higher-resolution
618 Version of the Max Planck Institute Earth System Model (MPI-ESM1.2-HR). *Journal of*
619 *Advances in Modeling Earth Systems* 10:1383–1413.
- 620 O’Neill, B. C., C. Tebaldi, D. P. Van Vuuren, V. Eyring, P. Friedlingstein, G. Hurtt, R. Knutti,
621 E. Kriegler, J. F. Lamarque, J. Lowe, G. A. Meehl, R. Moss, K. Riahi, and B. M. Sanderson.
622 2016. The Scenario Model Intercomparison Project (ScenarioMIP) for CMIP6.
623 *Geoscientific Model Development* 9:3461–3482.
- 624 Palazzi, E., L. Mortarini, S. Terzago, and J. von Hardenberg. 2019. Elevation-dependent
625 warming in global climate model simulations at high spatial resolution. *Climate Dynamics*
626 52:2685–2702.
- 627 Pierce, D. W., T. P. Barnett, B. D. Santer, and P. J. Gleckler. 2009. Selecting global climate
628 models for regional climate change studies. *Proceedings of the National Academy of*
629 *Sciences of the United States of America* 106:8441–8446.
- 630 Ribes, A., S. Qasmi, and N. P. Gillett. 2021. Making climate projections conditional on historical
631 observations. *Science Advances* 7:1–10.
- 632 Rupp, D. E., J. T. Abatzoglou, K. C. Hegewisch, and P. W. Mote. 2013. Evaluation of CMIP5
633 20th century climate simulations for the Pacific Northwest USA. *Journal of Geophysical*
634 *Research Atmospheres* 118:10884–10906.
- 635 Salathé, E. P., R. Steed, C. F. Mass, and P. H. Zahn. 2008. A high-resolution climate model for
636 the U.S. Pacific northwest: Mesoscale feedbacks and local responses to climate change.
637 *Journal of Climate* 21:5708–5726.
- 638 Sférian, R., P. Nabat, M. Michou, D. Saint-Martin, A. Voldoire, J. Colin, B. Decharme, C.
639 Delire, S. Berthet, M. Chevallier, S. Sénési, L. Franchisteguy, J. Vial, M. Mallet, E.

640 Joetzjer, O. Geoffroy, J. F. Guérémy, M. P. Moine, R. Msadek, A. Ribes, M. Rocher, R.
641 Roehrig, D. Salas-y-Mélie, E. Sanchez, L. Terray, S. Valcke, R. Waldman, O. Aumont, L.
642 Bopp, J. Deshayes, C. Éthé, and G. Madec. 2019. Evaluation of CNRM Earth System
643 Model, CNRM-ESM2-1: Role of Earth System Processes in Present-Day and Future
644 Climate. *Journal of Advances in Modeling Earth Systems* 11:4182–4227.

645 Sellar, A. A., C. G. Jones, J. P. Mulcahy, Y. Tang, A. Yool, A. Wiltshire, F. M. O’Connor, M.
646 Stringer, R. Hill, J. Palmieri, S. Woodward, L. de Mora, T. Kuhlbrodt, S. T. Rumbold, D. I.
647 Kelley, R. Ellis, C. E. Johnson, J. Walton, N. L. Abraham, M. B. Andrews, T. Andrews, A.
648 T. Archibald, S. Berthou, E. Burke, E. Blockley, K. Carslaw, M. Dalvi, J. Edwards, G. A.
649 Folberth, N. Gedney, P. T. Griffiths, A. B. Harper, M. A. Hendry, A. J. Hewitt, B. Johnson,
650 A. Jones, C. D. Jones, J. Keeble, S. Liddicoat, O. Morgenstern, R. J. Parker, V. Predoi, E.
651 Robertson, A. Siahann, R. S. Smith, R. Swaminathan, M. T. Woodhouse, G. Zeng, and M.
652 Zerroukat. 2019. UKESM1: Description and Evaluation of the U.K. Earth System Model.
653 *Journal of Advances in Modeling Earth Systems* 11:4513–4558.

654 Sherwood, S., M. J. Webb, J. D. Annan, K. C. Armour, P. M. Forster, J. C. Hargreaves, G.
655 Hegerl, S. A. Klein, K. D. Marvel, E. J. Rohling, M. Watanabe, T. Andrews, P. Braconnot,
656 C. S. Bretherton, G. L. Foster, Z. Hausfather, A. S. von der Heydt, R. Knutti, T. Mauritsen,
657 J. R. Norris, C. Proistosescu, M. Rugenstein, G. A. Schmidt, K. B. Tokarska, and M. D.
658 Zelinka. 2020. An assessment of Earth’s climate sensitivity using multiple lines of
659 evidence. *Reviews of Geophysics*:0–2.

660 Sutton, R. T. 2018. ESD Ideas: A simple proposal to improve the contribution of IPCC WGI to
661 the assessment and communication of climate change risks. *Earth System Dynamics*
662 9:1155–1158.

663 Sutton, R. T., and E. Hawkins. 2020. ESD Ideas : Global climate response scenarios for IPCC
664 assessments:751–754.

665 Swart, N. C., J. N. S. Cole, V. V. Kharin, M. Lazare, J. F. Scinocca, N. P. Gillett, J. Anstey, V.
666 Arora, J. R. Christian, S. Hanna, Y. Jiao, W. G. Lee, F. Majaess, O. A. Saenko, C. Seiler, C.
667 Seinen, A. Shao, M. Sigmond, L. Solheim, K. Von Salzen, D. Yang, and B. Winter. 2019.
668 The Canadian Earth System Model version 5 (CanESM5.0.3). *Geoscientific Model*
669 *Development* 12:4823–4873.

670 Tabor, K., and J. W. Williams. 2010. Globally downscaled climate projections for assessing the
671 conservation impacts of climate change. *Ecological Applications* 20:554–565.

672 Tatebe, H., T. Ogura, T. Nitta, Y. Komuro, K. Ogochi, T. Takemura, K. Sudo, M. Sekiguchi, M.
673 Abe, F. Saito, M. Chikira, S. Watanabe, M. Mori, N. Hirota, Y. Kawatani, T. Mochizuki, K.
674 Yoshimura, K. Takata, R. O’ishi, D. Yamazaki, T. Suzuki, M. Kurogi, T. Kataoka, M.
675 Watanabe, and M. Kimoto. 2018. Description and basic evaluation of simulated mean state,
676 internal variability, and climate sensitivity in MIROC6. *Geoscientific Model Development*
677 12:2727–2765.

678 Taylor, K. E., R. J. Stouffer, and G. A. Meehl. 2012. An overview of CMIP5 and the experiment
679 design. *Bulletin of the American Meteorological Society* 93:485–498.

- 680 Volodin, E. M., E. V. Mortikov, S. V. Kostykin, V. Y. Galin, V. N. Lykossov, A. S. Gritsun, N.
681 A. Diansky, A. V. Gusev, and N. G. Iakovlev. 2017. Simulation of the present-day climate
682 with the climate model INMCM5. *Climate Dynamics* 49:3715–3734.
- 683 Wang, K., and G. D. Clow. 2020. The diurnal temperature range in CMIP6 models: Climatology,
684 variability, and evolution. *Journal of Climate* 33:8261–8279.
- 685 Wang, T., A. Hamann, D. Spittlehouse, and C. Carroll. 2016. Locally downscaled and spatially
686 customizable climate data for historical and future periods for North America. *Plos One*
687 11:e0156720.
- 688 Wang, T., A. Hamann, D. L. Spittlehouse, and T. Q. Murdock. 2012. ClimateWNA: high-
689 resolution spatial climate data for western North America. *Journal of Applied Meteorology*
690 and *Climatology* 51:16–29.
- 691 Wilby, R. L., S. P. Charles, E. Zorita, B. Timbal, P. Whetton, and L. O. Mearns. 2004.
692 Guidelines for Use of Climate Scenarios Developed from Statistical Downscaling Methods.
693 Page IPCC Task Group on Data and Scenario Support for Impact and Climate Analysis
694 (TGICA).
- 695 Wilson, L. J., M. Vallee, and J. Montpetit. 2008. Comments on “Hydrometeorological Accuracy
696 Enhancement via Postprocessing of Numerical Weather Forecasts in Complex Terrain.”
697 *Weather and Forecasting* 24:892–894.
- 698 Wu, T., Y. Lu, Y. Fang, X. Xin, L. Li, W. Li, W. Jie, J. Zhang, Y. Liu, L. Zhang, F. Zhang, Y.
699 Zhang, F. Wu, J. Li, M. Chu, Z. Wang, X. Shi, X. Liu, M. Wei, A. Huang, Y. Zhang, and X.
700 Liu. 2019. The Beijing Climate Center Climate System Model (BCC-CSM): The main
701 progress from CMIP5 to CMIP6. *Geoscientific Model Development* 12:1573–1600.
- 702 Yukimoto, S., H. Kawai, T. Koshiro, N. Oshima, K. Yoshida, S. Urakawa, H. Tsujino, M.
703 Deushi, T. Tanaka, M. Hosaka, S. Yabu, H. Yoshimura, E. Shindo, R. Mizuta, A. Obata, Y.
704 Adachi, and M. Ishii. 2019. The meteorological research institute Earth system model
705 version 2.0, MRI-ESM2.0: Description and basic evaluation of the physical component.
706 *Journal of the Meteorological Society of Japan* 97:931–965.
- 707 Ziehn, T., M. A. Chamberlain, R. M. Law, A. Lenton, R. W. Bodman, M. Dix, L. Stevens, Y. P.
708 Wang, and J. Srbinovsky. 2020. The Australian Earth System Model: ACCESS-ESM1.5.
709 *Journal of Southern Hemisphere Earth Systems Science* 70:193–214.

710